Satellite-Derived Surface Radiation Budget over the African Continent. Part II: Climatologies of the Various Components

MAMOUDOU B. BA* AND SHARON E. NICHOLSON

Department of Meteorology, The Florida State University, Tallahassee, Florida

ROBERT FROUIN

Scripps Institution of Oceanography, University of California, San Diego, La Jolla, California

(Manuscript received 27 May 1999, in final form 9 March 2000)

ABSTRACT

The temporal and spatial variabilities of the surface radiation budget over the African continent are examined using Meteosat data acquired during 1983–88. Continental maps of land surface albedo, downward solar irradiance, and net radiation are presented for the midseasonal months of January, April, July, and October. Surface albedo is further compared with Special Sensor Microwave Imager polarization difference of brightness temperature at 19 GHz and with the normalized difference vegetation index to assess the results and to test proposed explanations for some of the unanticipated results. An example of the latter is the finding that albedo increases throughout most of the Southern Hemisphere and in the lower latitudes of the Northern Hemisphere during the wet season. Overall, the study demonstrates the complexity of the relationships among surface albedo, vegetation, and soils and underscores a strong interhemispheric contrast in radiation regimes.

1. Introduction

In Part I of this series (Ba et al. 2001), we described a methodology for deriving estimates of solar irradiance and surface albedo using Meteosat data and compared our results with those of other investigators. Here in Part II, the methodology is applied to studying the radiation balance of the African continent.

The results have several potential applications because of the importance of surface solar irradiance at the surface in driving the global climate system. It is the primary energy source for the system and controls the surface energy balance. It is also the key factor governing primary productivity of vegetation. For this reason, accurate estimates of surface radiation balance are necessary for climate modeling. Likewise, accurate estimates of surface albedo are needed, particularly in general circulation models (GCMs). Although GCMs require surface albedo estimates with an accuracy ranging from 0.01 to 0.05 on the monthly timescale, most GCMs currently use inaccurate maps of surface albedo and/or adopt a typical albedo value for a given vegetation class. It would be preferable to map surface albedo over long time periods, possibly over several spectral bands, and to develop models of surface albedo variation as a function of vegetation type and seasonal evolution. This can be done only via satellites.

For the African continent, albedo is of special interest because of the hypothesis of Charney (1975) and others that increased surface albedo, accompanying drought of human-induced desertification, might exacerbate or even trigger drought. Numerous satellite estimates of surface albedo have been made over West Africa (e.g., Norton et al. 1979; Courel et al. 1984; Pinty et al. 1985; Pinty and Szejwach 1985; Deschamps and Dedieu 1986; Pinty and Tanré 1987; Pinty and Ramond 1987). Fewer estimates of continental-scale albedo have been made, notably those of Li and Garand (1994), Pinker and Laszlo (1992), and Darnell et al. (1992). While most have emphasized methodologies, Norton et al.(1979) and Courel et al.(1984) have examined the seasonal and interannual variations in an attempt to evaluate Charney's hypothesis.

The aim of this paper is to describe temporal and spatial variations of downward solar irradiance and surface albedo over Africa as deduced from satellite estimates for the period of 1983–88. A study of surface net radiation is also presented using complementary data on surface net longwave radiation estimates obtained

* Current affiliation: Department of Meteorology, University of Maryland, College Park, Maryland.

Corresponding author address: Dr. Mamoudou B. Ba, Department of Meteorology, University of Maryland, College Park, MD 20742. E-mail: mba@atmos.umd.edu

from National Aeronautics and Space Administration (NASA) Langley Research Center Distributed Active Archive Center (DAAC) (Gupta et al. 1999). First, we focus on the regional and seasonal distribution of these three surface radiation budget (SRB) parameters. Then, we examine their interannual variability during the period of study using longitudinal transects at 10°W and 19°E. Finally, the relationship between albedo and surface characteristics is analyzed using vegetation index and Special Sensor Microwave Imager (SSM/I) polarization difference of brightness temperature at 19 GHz (hereinafter referred to as PD19). The results depict the complexity of the albedo–vegetation relationship and also underscore the interhemispheric contrast in surface albedo over Africa.

2. Data

Multiyear Meteosat visible near-infrared data and climatologies of vertically integrated water vapor content (Tuller 1968) and vertically integrated ozone content (London et al. 1976) are used for the present study. A constant aerosol optical thickness of 0.23 is used in the computation of solar downward irradiance and surface albedo, as described in Part I. Surface net longwave radiation estimates obtained from DAAC are also used to compute surface net radiation. The DAAC datasets are mapped to the International Satellite Cloud Climatology Project (ISCCP) equal-area grid, which approximates dimensions of 278 km × 278 km (2.5° latitude × 2.5° longitude). The downward solar irradiance and surface albedo obtained from Meteosat visible channel (0.4–1.1 μm) are computed at 0.25° × 0.25°, but we preferred to utilize a 1° × 1° spatial resolution for maps shown in the following sections in order to have a smoother field for easier analysis. To compute the surface net radiation, Meteosat products (downward surface solar irradiance and albedo) are degraded by averaging all the 30-km pixels contained within a 2.5° grid box to match the 280-km resolution of the ISCCP C1 data.

3. Downward surface solar irradiance

a. Seasonal variations

Figure 1 presents the continental distribution of the monthly mean downward surface solar irradiance at a spatial resolution of 1° latitude × 1° longitude for the months of January, April, July, and October. The monthly mean means are averaged from 1983 to 1988. The January field (Fig. 1a) is characterized by a nearly zonal distribution over northern Africa above 10°N with values that do not exceed 225 W m^{-2}. Values exceeding 250 W m^{-2} prevail between 0° and 10°N. The equatorial regions of southern Africa are characterized by values ranging from 225 to below 200 W m^{-2}. Over southwestern Africa (Namibia), the surface downward solar irradiance exceeds 300 W m^{-2}.

During April (Fig. 1b), irradiance ranges from 275 to 300 W m^{-2} along the northern and southern boundaries of the Sahara; peak values in the central Sahara exceed 300 W m^{-2}. In the equatorial regions of southern Africa, where irradiance does not exceed 225 W m^{-2}, there is little spatial variation.

During July, irradiance is still high over the Sahara, exceeding 325 W m^{-2} in the northern desert (see Fig. 1c), but a seasonal minimum is reached in southern Africa. In Sahelo–Soudanian regions, irradiance is decreased, a consequence of increasing cloudiness associated with the migration of the intertropical convergence zone (ITCZ) to the north. The field remains nearly zonal over these regions and shows a relatively high north–south gradient. Irradiance is reduced to less than 200 W m^{-2} over the Guinean coast and Cameroon.

In October (Fig. 1d), the maxima lie over the Sahel and southwestern Africa. The lowest values are found over the equatorial regions and the northernmost and the southernmost parts of the continent. Nowhere does irradiance exceed 300 W m^{-2}.

b. Interannual variability

The interannual variability of downward solar irradiance is primarily due to changes in atmospheric conditions (cloudiness, water vapor, and aerosol content). Clouds are an especially important determinant of the downward shortwave flux, as they strongly attenuate the incoming radiation. Latitudinal transects of downward solar irradiance for January and July illustrate the interannual variability during the period of 1983–88. Figure 2 presents transects at 10°W (top) and at 19°E (bottom).

These transects indicate that the interannual variability of downward solar irradiance is relatively small, although some years do stand out. One of these is 1985, a year when January irradiance is clearly lower at 10°W than during the other years by as much as 50 W m^{-2}. Examination of the infrared images for that month showed the presence of a persistent cloud band stretching from the Atlantic coast of Senegal to the Mediterran coast of Libya. Such diagonal cloud bands do occur on occasion in this region and may even bring up to 25 mm of rainfall in areas where January is generally absolutely dry (Flohn 1971; Nicholson 1981). However, they are relatively unusual.

If the anomalous pattern associated with 1985 is ignored, the transects show three general trends. The first is that the interannual variability is somewhat greater in the wet season than in the dry season. The second is that the lowest interannual variability is over the southern Sahara and the semiarid zone south of it, in the latitudes from roughly 16° to 22°N. The third is that interannual variability is generally high near the ITCZ. Thus, it is large in July south of 15°N at 10°W and from 2° to 12°N at 19°E.

At 10°W in January the interannual variability is rel-

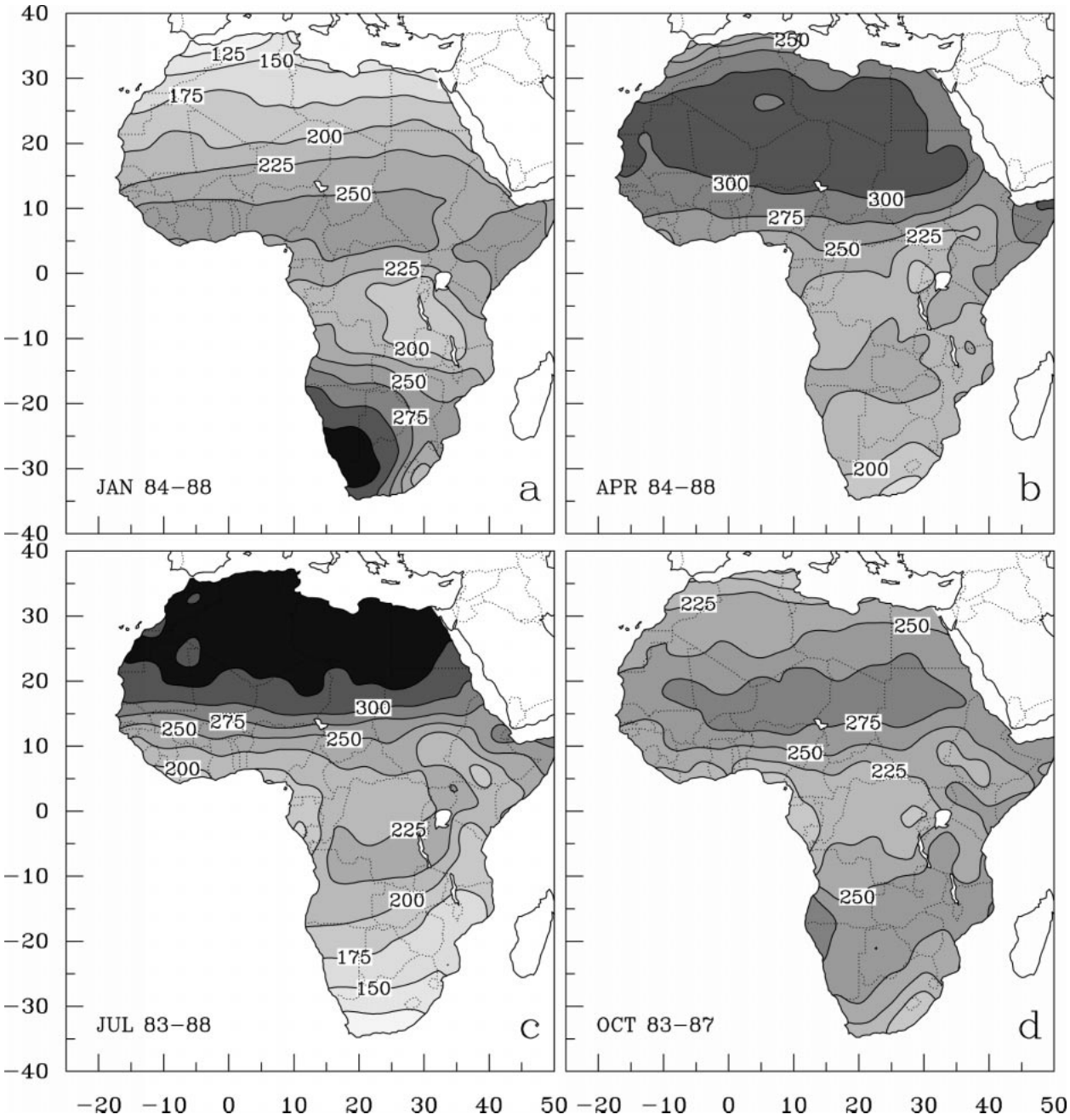

FIG. 1. Distribution of downward solar irradiance (W m^{-2}) for (a) Jan, (b) Apr, (c) Jul, and (d) Oct.

atively small (from 10 to 15 W m^{-2}) in the latitudes from 8° to 22°N. In this region, January is usually absolutely dry. Interannual variability increases with latitude (as does rainfall) north of 22°N, where the midlatitude winter rainfall regime commences. The range of January values is nearly 50 W m^{-2} at 30°N. In July, interannual variability is notably higher than in January in the latitudes from 8° to 15° or 16°N, where July is one of the wettest months.

The transect at 19°E underscores the contrast between the wet and dry seasons. In January, interannual variability is high south of the equator (where January is part of the wet season) and north of 22°N, an arid region that is most likely to receive its meager rainfall in winter. In July, there is a clear maximum between 2° and 16°N, where July is generally a wet month.

One surprising feature in the 19°E transect is the relatively high interannual variability in the latitudes from 2° to 12°S, latitudes that generally experience yearround rainfall. Much of the variance is due to the anom-

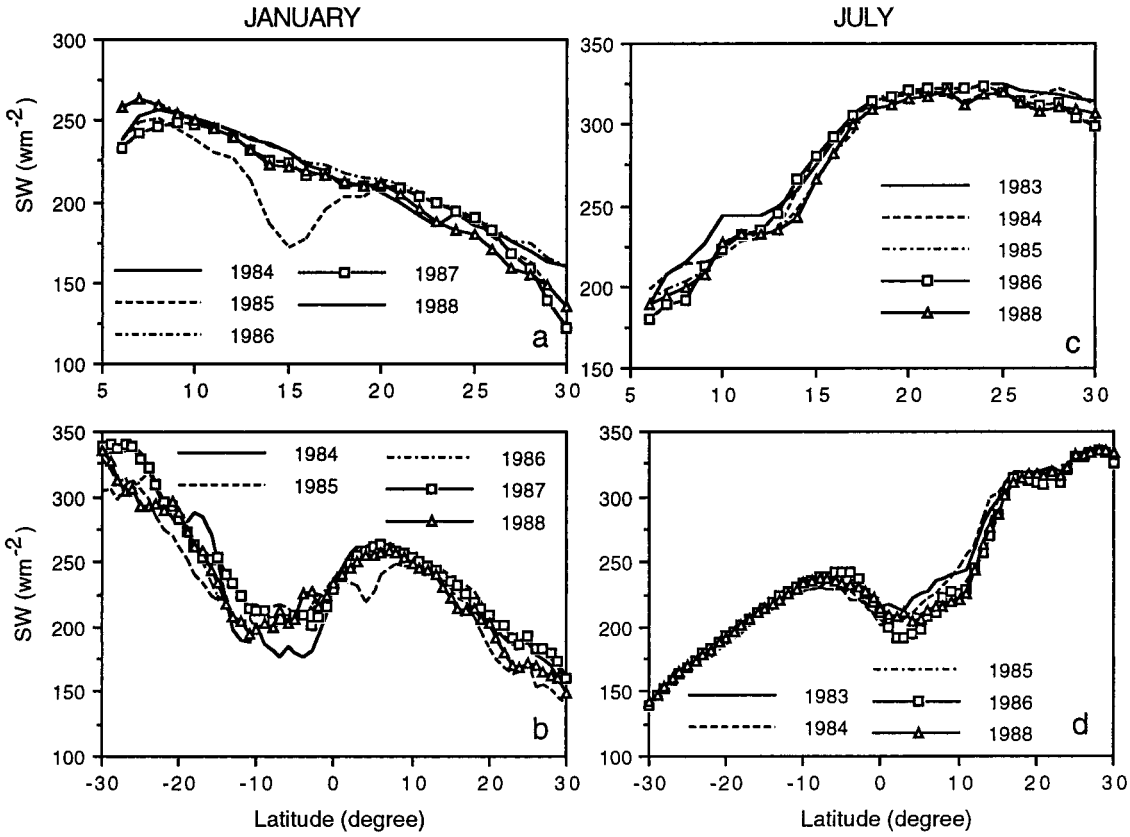

FIG. 2. Interannual variation of downward solar irradiance (W m^{-2}) for north–south transects at (top) 10°W and at (bottom) 19°E for (left) Jan and (right) Jul.

alous cloudiness of the January 1984 anomaly within this band, but the range is relatively large during the remaining years as well. This suggests significant interannual variability in cloudiness, an idea that is counter to the common perception of a relatively constant climatological regime in equatorial regions. It is also noteworthy that the interannual variability of solar radiation is somewhat higher in the low-latitude regions of the Southern Hemisphere than in those same latitudes in the Northern Hemisphere. This is surprising in view of the extreme year-to-year variability of rainfall in regions such as the Sahel. However, this result is consistent with an analysis of surface-based cloud estimates in the Sahel that showed little contrast between wet and dry years (Lare and Nicholson 1990).

4. Surface albedo

a. Spatial aspects

Figure 3 represents the continental distribution of the monthly mean surface albedo (1983–88) at a spatial resolution of 1° latitude × 1° longitude for four individual months, each representing a season. Similar maps were also obtained for the other months of the year but are not presented here. These show a large range of albedo, from low values in equatorial Africa that do not exceed 0.20 to values exceeding 0.50 in some desert regions of the subtropics. Values in the Sahel of West Africa exhibit a strong zonal character, but this is generally not the case elsewhere over the continent.

The most prominent features of the geographical pattern of surface albedo are the maxima over the Sahara Desert and the Kalahari Desert. These features are relatively invariant throughout the year. In three desert regions, surface albedo reaches 0.50 during all or most of the year. These are in the eastern part of Mauritania at its border with Mali, the central Algerian Sahara, and the Ténéré Desert located north-northwest of Lake Chad. A comparison with maps of soils (e.g., FAO 1977) and Saharan sand seas shows that the variations of surface albedo over the Sahara correspond to identifiable surface features and discontinuities. The areas of highest albedo correspond to the Great Sand Seas of the Grand Erg Oriental, the Majabat al Koubra, Fachi-Bilma, and Ténéré (Fig. 4). A fourth area of high albedo (exceeding 0.40 or 0.45) corresponds to the sand seas of the eastern Sahara. For the most part, these sand seas are areas where the FAO map indicates solonchaks (highly reflective saline soils), although these are weakly developed. Minimum albedo is evident over the mountainous

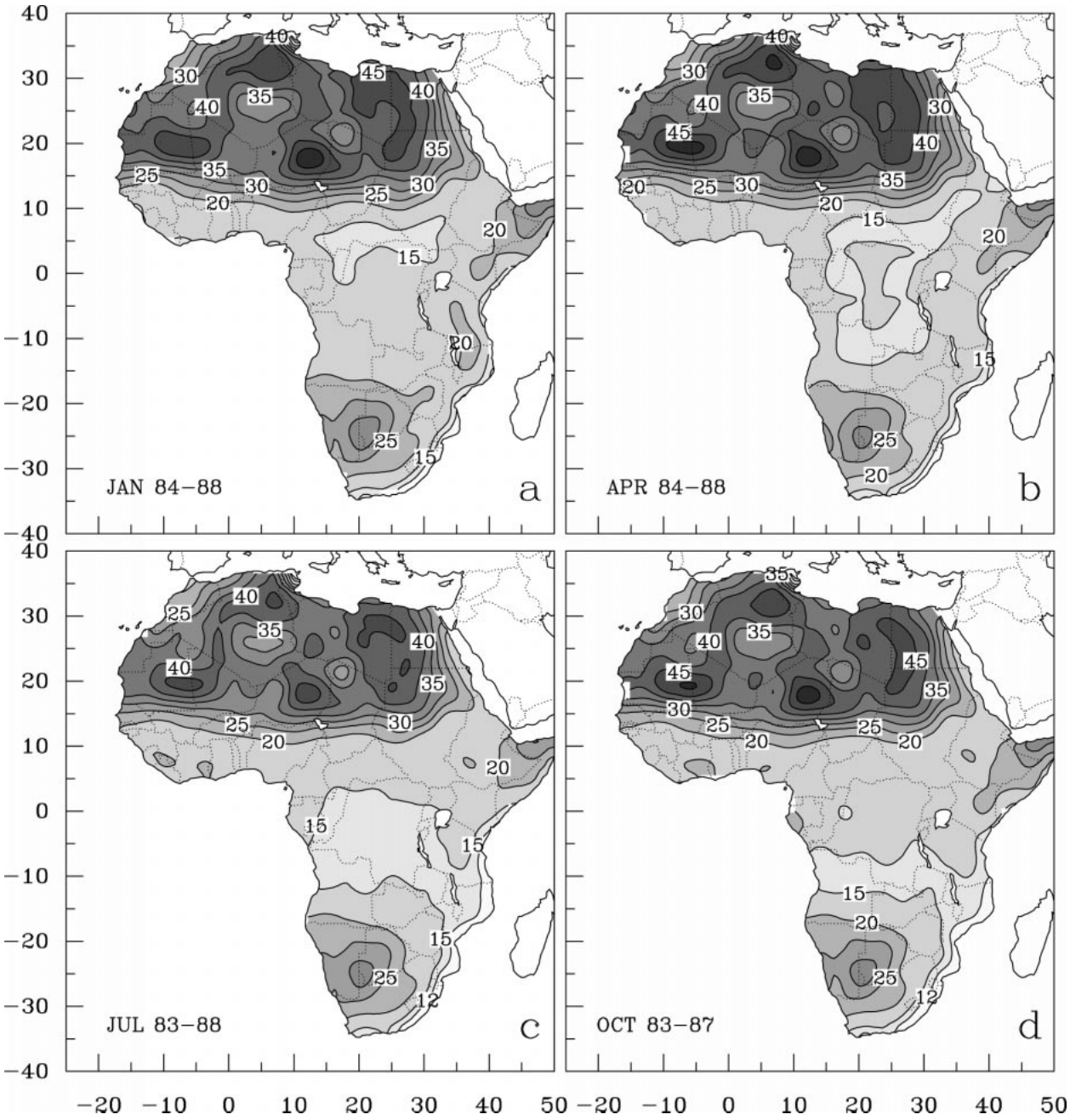

FIG. 3. Distribution of surface albedo (%) for (a) Jan, (b) Apr, (c) Jul, and (d) Oct.

areas of Tibesti and the Hoggar. Albedo is also relatively low over the less extreme highlands of Air and Tanezrouft Iforas. In these regions, the soils are indicated as weakly developed leptosols that occasionally sustain sparse vegetation. This suggests that over the Sahara, the surface reflectivity is strongly dependent on surface features.

Over West Africa, from the southern Sahel near 12°N to the central desert regions of Mali and Mauritania, our estimates range between about 0.20 and 0.50, being somewhat lower in July than in January. Within this same area, the estimates of Pinty and Ramond (1987) range from about 0.20 to 0.50, and those of Li and Garand (1994) range from 0.15 to 0.45. In the northern Sahelian zone, from 18° to 20°N and from 2° to 10°W, our albedo averages are 0.45 for January and 0.44 for July, compared to 0.44 and 0.46 estimates for February and July 1979, by Pinty and Ramond (1987). These are also in relatively good agreement with early assessments by Courel et al. (1984) (ranging from 0.40 to 0.50) and

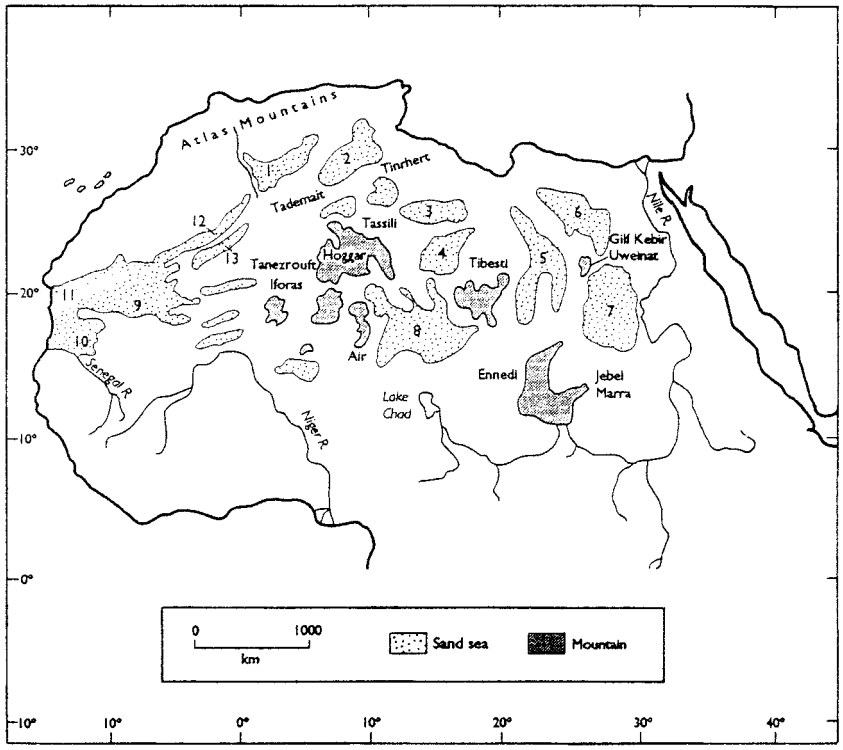

FIG. 4. The major physiographic features of the Sahara [from Lancaster (1996)]. Major sand seas: 1, Grand Erg Occidental; 2, Grand Erg Oriental; 3, Ubari; 4, Murzuk; 5, Calanscio; 6, Great Sand Sea; 7, Selima; 8, Fachi-Bilma and Ténéré; 9, Majabat al Koubra; 10, Aouker; 11, Akchar; 12, Iguidi; 13, Chech.

Rockwood and Cox (1978) (0.42 or greater) based on Meteosat and SMS data, respectively. Of note is the strong gradient in surface albedo, with values increasing from 0.20 to 0.40 within 5 degrees of latitude over the western Sahel.

In equatorial regions, from 10°N to 10°S, our values are generally on the order of 0.14 to 0.20 in both January and July and are in good agreement with those of Li and Garand (1994). Over semiarid regions of southern Africa, our estimates range from 0.15 to 0.30 over most of the region, likewise in agreement with the results of Li and Garand (1994). A comparison with the albedo over the Sahel, noted above, indicates that surface albedo in semiarid regions of southern Africa is significantly lower than over the semiarid western Sahel. The spatial gradients of albedo are also comparatively weak, with the maximum being a change from 0.15 to 0.25 within 10 degrees of latitude in the far southwest.

b. Direct comparison with results of other studies

Because of its importance in the context of drought and desertification, surface albedo in the West African Sahel has been intensively studied. Several studies afford an excellent opportunity for direct comparison with our results at individual locations in the country of Burkina Faso located in the southern Sahel (Table 1). These include Pinty and Tanré (1987), Deschamps and Dedieu (1986), and Pinty and Ramond (1987). Pinty and Tanré (1987) used measurements of downward surface solar irradiance together with Meteosat radiances to derive the mean albedo on 18 February and 2 July 1979. Pinty

TABLE 1. Mean surface albedo over three different sites in Burkina Faso.

	Pinty and Raymond (1987)		Deschamps and Dedieu (1986)		Pinty and Tanré (1987)	This study		
Sites	Feb 1979	Jul 1979	Jul 1983	Jul 1984	Jul 1979	Jul 1983	Feb 1984	Jul 1984
Dori (14.05°N, 0°)	0.34	0.29	0.26	0.26	0.29	0.29	0.37	0.28
Ouagadougou (12.42°N, 0°)	0.25	0.22	0.21	0.21	0.23	0.19	0.29	0.19
Fada Ngourma (12.06°N, 0.4°E)	0.24	0.23	0.20	0.20	0.22	0.18	0.25	0.19

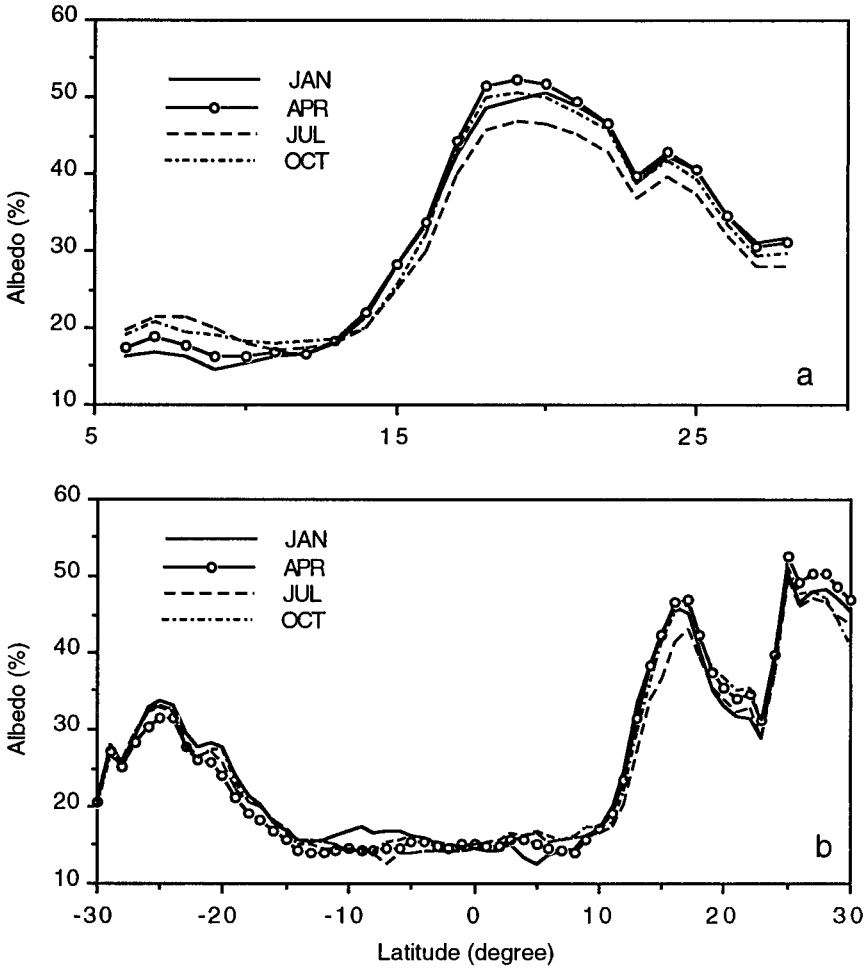

FIG. 5. Seasonal variation of surface albedo (%) for north–south transects at (a) 10°W and at (b) 19°E for the midseasonal months of Jan (solid line), Apr (dotted line), Jul (dashed line), and Oct (dashed–dotted line).

and Ramond's (1987) values are surface albedo estimates corrected for atmospheric and angular effects using Meteosat data obtained near the local noon on 18 February and 2 July 1979. Deschamps and Dedieu's values are reflectances computed at 1130 UTC. These comparisons are for different spectral ranges (e.g., 0.3–3.0 μm for Pinty and Raymond (1987) and Pinty and Tanré (1987) and 0.4–1.1 μm for Descahmps and Dedieu (1986) and for the present study. For vegetation and bare soil, a simulation using the Simulation of the Satellite Signal in the Solar Spectrum (5S; Tanré et al. 1990) shows that the surface albedo in the 0.4–1.1-μm spectral range is typically 0.277 and 0.195, respectively. These values compare with 0.265 and 0.211 in the total solar spectrum (0.25–4.0 μm). The differences are small ($<$10%) and may be even smaller for ''mixed'' pixels.

Generally, our values agree well with those obtained by all three investigators mentioned above (Table 1). Our February values are somewhat higher than those obtained by Pinty and Ramond at Dori and Ouagadougou. During July, our estimates are generally lower than those obtained by the others for Ouagadougou and Fada Ngourma. Although our estimates and those of Pinty and Ramond are made for different years, they are the most comparable because both represent the daily mean surface albedo. Those obtained by Deschamps and Dedieu and those of Pinty and Tanré are surface albedo obtained at one point in time near the local noon.

c. Latitudinal and seasonal variations

The large-scale, season-to-season changes in surface albedo are apparent in the maps described in section 4a (Fig. 3), as are the latitudinal variations. However, both the seasonal changes and the latitudinal gradients, particularly their magnitudes, are better depicted using north–south transects of surface albedo for four individual months (Fig. 5) and a seasonality index (Fig. 6).

At 10°W (Fig. 5a), surface albedo ranges from about 0.16 to 0.22 in the latitude band from 6° to 13°N, with

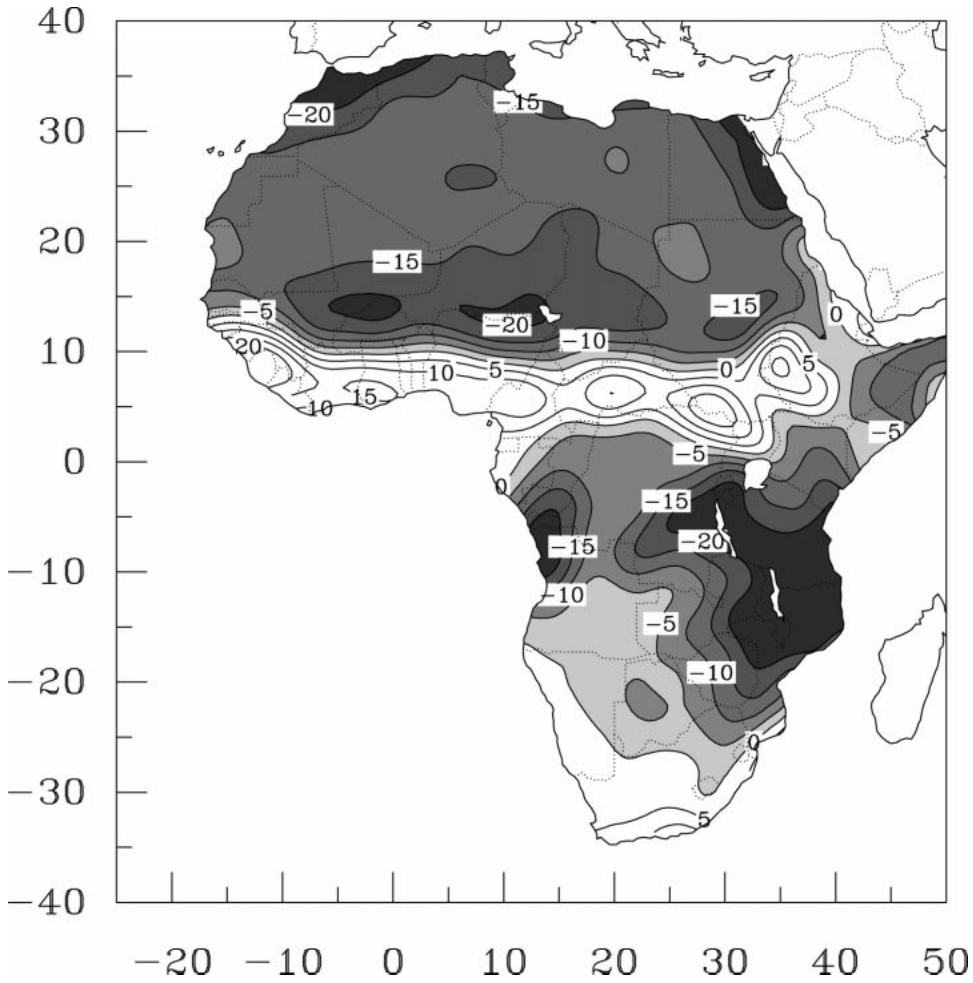

FIG. 6. Seasonality index (*S*) of surface albedo. Expressed in percent, *S* represents the difference between values of Jul and Feb normalized by that of Feb.

minimum values from 11° to 13°N for July and October. It increases abruptly from 0.18 at 13°N to 0.50 at 18°N, then shows a broad maximum centered around 20°N. From there northward to 28°N, it shows a relatively steady decrease to about 0.32. A weak secondary minimum appears near 23°N.

The transect at 19°E (Fig. 5b) is interesting because it allows one to compare the gradients of surface albedo between arid and semiarid regions of Northern and Southern Hemispheres. In the Southern Hemisphere, surface albedo decreases steadily from the arid subtropics near 25°S, where it is about 0.33, to the humid equatorial zone, where it is roughly 0.15 throughout the area between 15°S and 0°. In the Northern Hemisphere, surface albedo is likewise about 0.15 in the equatorial latitudes, but from 10°N, it increases sharply to a maximum of nearly 0.50 around 15°–17°N. Thus, the latitudinal gradient in the Northern Hemisphere is considerably greater than in the Southern Hemisphere, most likely a consequence of a steeper rainfall gradient. The lower albedo over the Southern Hemisphere corresponds to a denser vegetation cover and wetter climate, with no desert region equivalent to the Sahara.

Farther north (i.e., in the latitudes between 20° and 24°N), surface albedo decreases to about 0.35, then increases to over 0.50 in the latitudes from 25° to 30°N. The low values from 20° to 24°N represent the Tibesti massif. Vegetation is somewhat greater here, as rainfall is significantly higher than in the surrounding lower plain. The topography itself might also influence the apparent surface albedo, and the aerosol effect is lower here than elsewhere in the Sahara and Sahel.

Seasonal variations are readily apparent from these transects. At 10°W, there are significant seasonal variations south of 12°N, with surface albedo slightly exceeding 0.15 in January and April and reaching 0.20 during July and October. Near 13°N, the seasonal cycle approaches zero, then reverses farther north. The amplitude of the seasonal cycle of albedo is surprisingly small within the semiarid regions from about 13° to

17°N but particularly large from about 18° to 22°N. This latter result is questionable, as there is little change in vegetation cover in this sector during the course of the year. It will be further considered in section 7.

At 19°E, a somewhat different picture emerges. In the Northern Hemisphere, there is a similar reversal of the seasonal cycle of albedo near 10°N, but a corresponding reversal is not apparent in the Southern Hemisphere. As would be expected, the amplitude of the cycle is near zero close to the equator but large in the outer tropical latitudes (near 12°–14°N and 5°–10°S), which experience well-defined dry and wet seasons. This is the case in both hemispheres. In contrast, the seasonal cycle is near zero over the desert regions in both hemispheres, except to the north of 25°N.

The seasonal cycle of albedo is further examined using a seasonality index (S) of surface albedo, defined as

$$S = \frac{100(\mathrm{As}_{\mathrm{jul}} - \mathrm{As}_{\mathrm{feb}})}{\mathrm{As}_{\mathrm{feb}}}, \quad (1)$$

where $\mathrm{As}_{\mathrm{jul}}$ and $\mathrm{As}_{\mathrm{feb}}$ refer to July and February surface albedo, respectively. February is used instead of January, as it better depicts the extremes in some parts of the Southern Hemisphere. Figure 6 presents a map of this index. This confirms the patterns seen in the transects and shows the generality of these results for the continent as a whole. The amplitude of the cycle is lowest in the equatorial latitudes, with nearly year-round rainfall, and in the desert regions of southwestern Africa. It is largest in the outertropical latitudes. The relatively small amplitude in these latitudes at 10°W, as noted earlier, is an anomaly related to the far northward extension of the wetter climates over the Guinean highlands and local surface hydrological conditions. Further evident are reversals in the sign of the seasonal cycle at 10°–13°N and 0°–4°N.

Overall, a somewhat surprising picture of surface albedo emerges from the transects and the seasonality index. At both 10°W and 19°E, the seasonal variation of surface albedo reverses north and south of about 13° and 10°N, respectively. To the north, minimum surface albedo corresponds to the wet season, maximum albedo to the dry season, as would probably be anticipated. However, the opposite is true to the south, with higher surface albedo during the wet season. In the Southern Hemisphere, maximum albedo also coincides with the wet season, with the minimum occurring at the end of the wet season and during the dry season.

Because directional effects due to changing solar geometry are minimized by using a directional function to normalize the data (see Part I), most of the seasonal changes in surface albedo in the vegetated regions are due to changing plant phenology. The result that maximum albedo corresponds to the wet season in some latitudes may relate to the peculiar spectral signature of vegetation, with vigorous green vegetation having a very high albedo at infrared wavelengths (Dickinson 1983). This would mean that in the case of a reasonably sparse cover with considerable bare ground exposed, albedo is high during the dry season, when soil is exposed and soil moisture is at a minimum. Such a situation occurs in the Sahel, where dry-season brushfires may further enhance this effect (Leroux et al. 1994). For a region with relatively dense cover, the vigor of the vegetation would govern the albedo, with the infrared effect being dominant and producing high albedos during the growth season. This is clearly the case in wet equatorial latitudes with forests and relatively dense woodlands. It is probably true of the southern semiarid Tropics as well, since vegetation density there is considerably higher than in the Sahel, despite similar conditions of rainfall (Nicholson and Farrar 1994). These ideas are further tested in section 7.

d. Interannual variability

The interannual variability of surface albedo reflects changes in surface properties, particularly in vegetation cover. Therefore, one may expect larger variability in regions, such as the Sahel, where the interannual variability of rainfall is much higher than elsewhere on the continent. In contrast, one should expect a lesser interannual variability over the Sahara.

Figure 7 illustrates the interannual variability of surface albedo for January 1984–88 (left-hand side) and July 1983–88 (right-hand side) for latitudinal transects at l0°W (top) and at 19°E (bottom). These transects do not show the anticipated patterns of surface albedo. For example, in the Saharan latitudes, there is a high degree of interannual variability that might be attributed to year-to-year changes in aerosol content, a factor insufficiently accounted for in the approach taken to atmospheric corrections (Part I). In the Sahelian region (cf. 12°–17°N at 10°W, 11°–15°N at 19°E), variability is relatively high in July, as might be anticipated from the extreme interannual variability of rainfall in the region. However, it is no larger than in the lower latitudes or in the equivalent latitudes of the Southern Hemisphere. Also, the interannual variability is relatively large throughout the Southern Hemisphere during both July and January. This is a puzzling result because south of 10° or 15°S, July is virtually rainless in all years. However, there may be variations in residual vegetation at the end of the season or in decaying vegetal matter on the surface.

Although the absolute magnitude of the interannual variability of surface albedo does not vary considerably with latitude, the relative magnitude does. In the desert, the difference between maximum and minimum values is generally less than 5% of the monthly mean, while in tropical latitudes (15°N–15°S), it can be as much as 35%–40% of the monthly mean (Fig. 7).

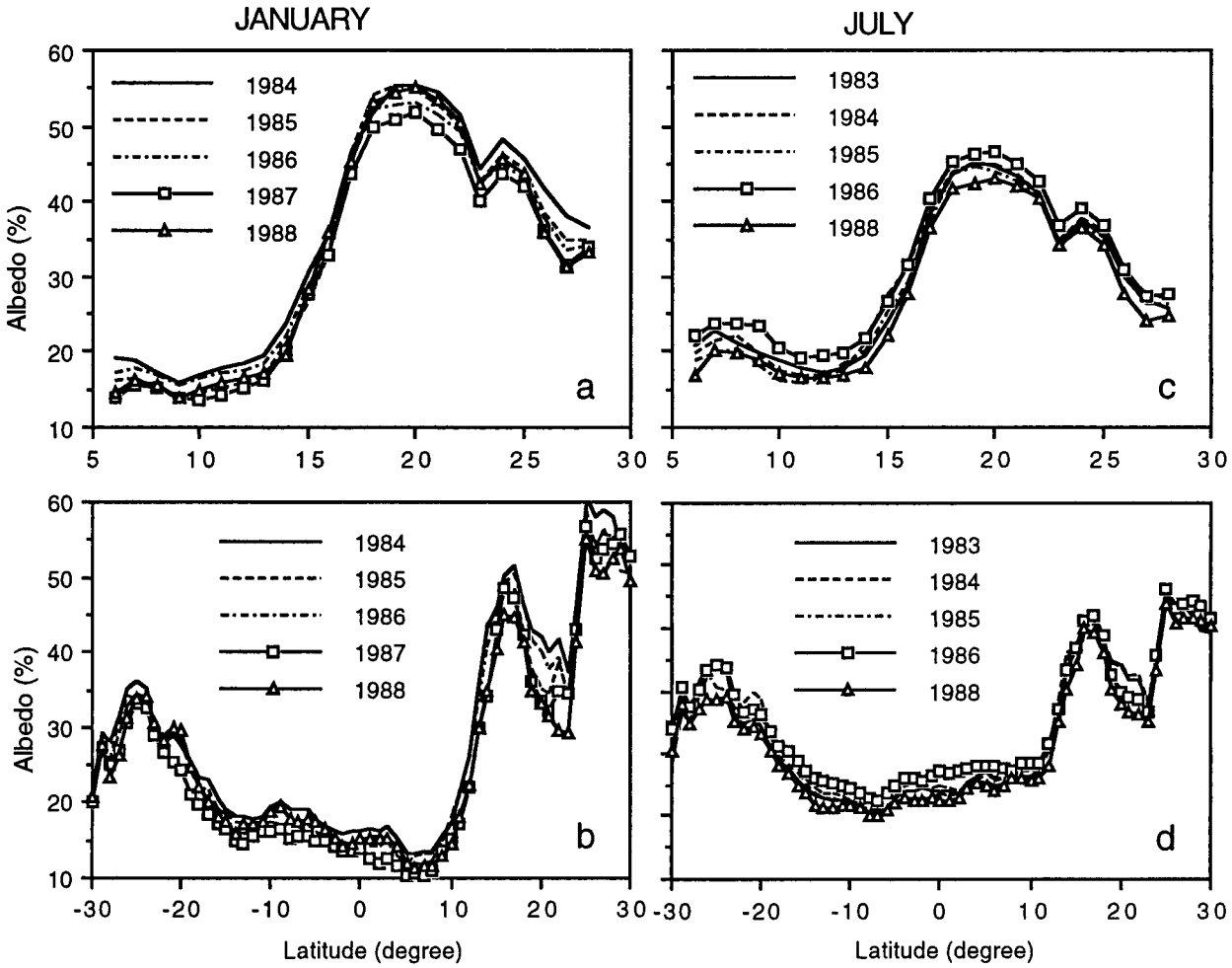

FIG. 7. Interannual variation of surface albedo (%) for north–south transects at (top) 10°W and at (bottom) 19°E for (left) Jan and (right) Jul.

5. Surface net radiation

a. Seasonal variations

To study the seasonal and interannual variations of net radiation, we combined our surface radiation estimates with DAAC longwave radiation estimates. Figure 8 shows the continental distribution of the monthly mean surface net radiation at a spatial resolution of 2.5° × 2.5° for the individual months of January, April, July, and October. As expected, the pattern of net radiation shows that over northernmost and southernmost Africa the minima (less than 25 W m^{-2}) occur in January and July, respectively. This results from reduced incoming solar radiation during January over northern Africa and during July over southern Africa.

The pattern of net radiation shows that the maximum (more than 150 W m^{-2}) occurs over the equatorial regions located between 10°N and 10°S. Values higher than 150 W m^{-2} dominate the April field over these regions (Fig. 8b), with a peak maximum of 175 W m^{-2} over the Guinean coast and Cameroon. During July, the peak maximum, exceeding 150 W m^{-2}, moves toward the north and is centered around 10°N. During October, peaks of maximum values exceeding 150 W m^{-2} are located in the equatorial regions (Fig. 8d).

b. Interannual variability

For January, some similarities are apparent with the patterns of surface downward irradiance. Examples are the anomalously low values in 1985 at 10°W and in 1984 at 19°E (Fig. 9). Also, for both downward irradiance and net radiation, highest values were for 1986 at many latitudes at 20°W (see Fig. 2a and Fig. 9a).

During July, variations of the surface net radiation from one year to another are generally small for the 10°W transect, except for 1988 (Fig. 9c). Values of the surface net radiation are generally much higher during July 1988 than any other year, especially between 15° and 25°N at 10°W (Figs. 9c and 9d). These high values are due to much higher values of DAAC net longwave radiation estimates (not shown here). These systematic

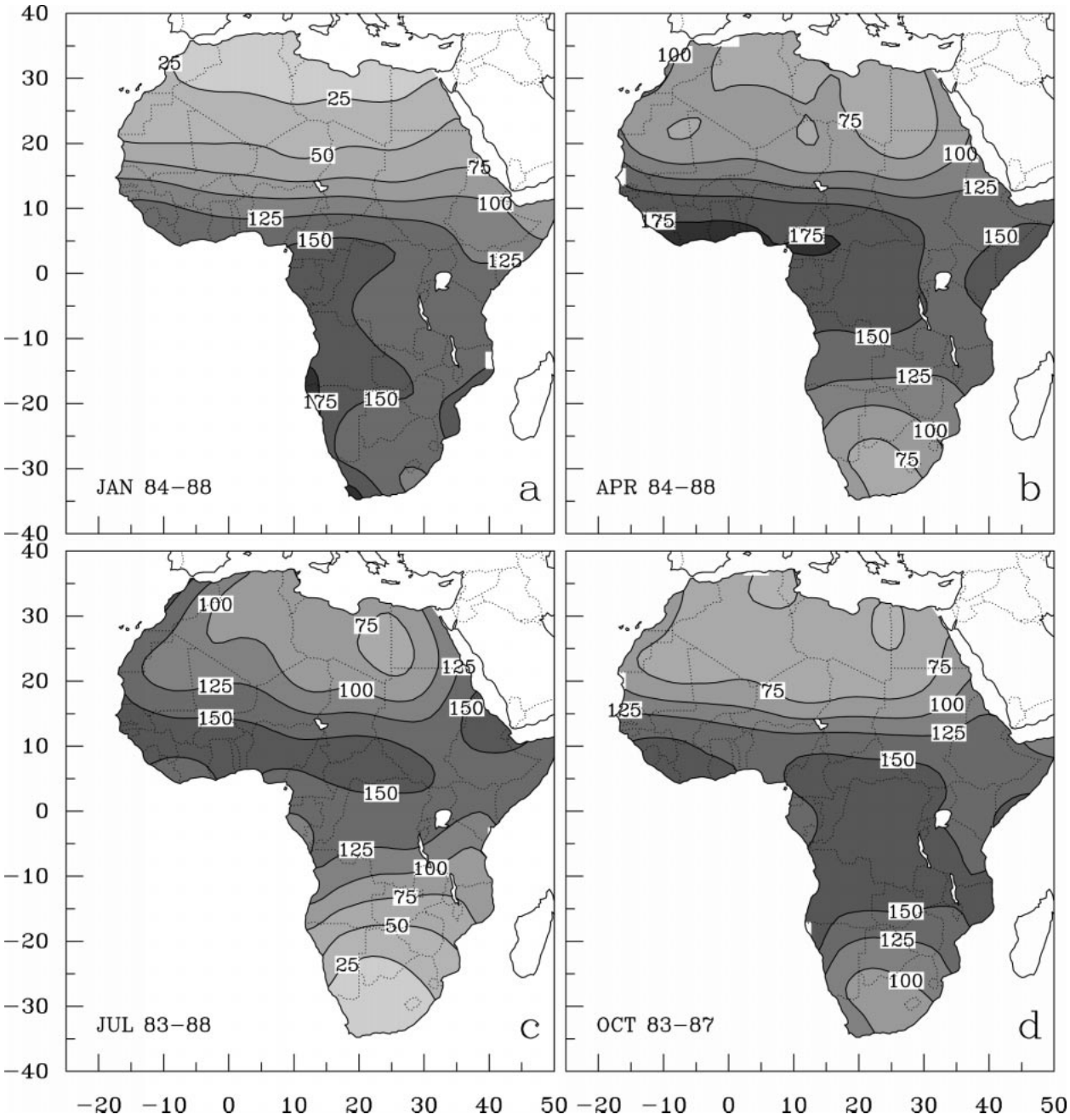

FIG. 8. Distribution of surface net radiation (W m^{-2}) for (a) Jan, (b) Apr, (c) Jul, and (d) Oct.

high estimates of net longwave radiation during July 1988 are questionable.

6. Comparison with climatological estimates of surface radiation balance

Prior to the availability of satellite data, surface radiation balance components were calculated from vegetation–albedo relationships and from empirical formulas governing atmospheric effects. Many studies, particularly those relating vegetation and surface energy balance, are based on so-derived data. Examples of the approach are given in Henning (1989), perhaps the most comprehensive treatment of surface heat balance on a continental basis. This work also underscores the wide diversity of ''traditional'' calculations by various methods, such as classic approaches by Penman, Albright, and Budyko. A broad comparison of our results with those presented by Henning reveals considerable discrepancies.

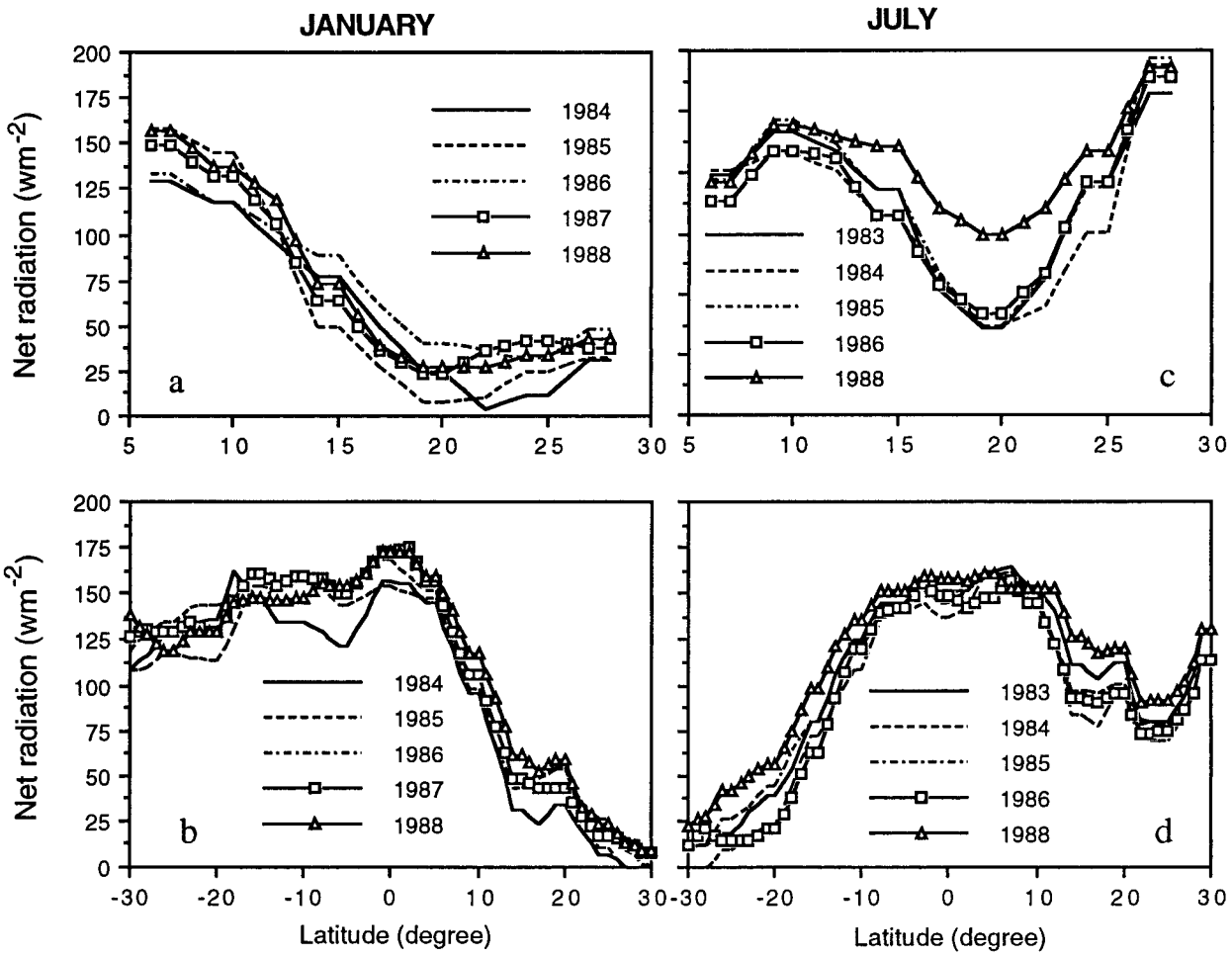

FIG. 9. Interannual variation of surface net radiation (W m^{-2}) for north–south transects at (top) 10°W and at (bottom) 19°E for (left) Jan and (right) Jul.

A comparison with surface albedo is difficult, because values in excess of 0.27 are not indicated. In general, however, in desert areas where values on the order of 0.25 are given, our analysis generally indicates 0.35–0.40. In humid equatorial regions where similar values are given, our analysis gives values on the order of 0.15–0.20. In the drier regions of the Southern Hemisphere, both sets of values are in rough agreement during both the dry and wet seasons, but in the more tropical latitudes of the Southern Hemisphere, ours are considerably lower during the dry season, less than 0.15 as compared with 0.15–0.25 in the Henning analysis.

These discrepancies clearly have an impact on net radiation, also presented by Henning in map form. However, the differences in net radiation in the two analysis are even more striking. Even the spatial configurations are quite diverse. For example, in December, Henning's map shows strongly zonal values with a general increase from the extreme north of Africa to the extreme south. The range extends from near 0 to about 200 W m^{-2}. In our analysis, there is a pronounced maximum in the low latitudes during January (the most comparable month), with values generally not exceeding 175 W m^{-2} and mostly falling in the range of 125–150 W m^{-2}. In July, the Henning map shows a general decrease in surface net radiation from about 150 W m^{-2} at the northern extreme of Africa to 0 at its southern. Ours also indicates a reversal in the pattern between January and July, but the result is a strong low-latitude maximum center at about 5°N. Values are about 75–100 W m^{-2} in the northernmost latitudes and less than 25 W m^{-2} in the southernmost latitudes. Consequently, throughout the continent the two sets of values may differ by factors of 2 or 3. This puts into question such accepted relationships as the one given by Budyko (1986) between net radiation (i.e., dryness ratio), rainfall, and vegetation biomes.

7. Discussion

The results of our study of surface albedo, particularly its seasonal variations, produced some rather surprising

results. These include a relatively pronounced seasonal cycle in some desert regions, the occurrence of maximum albedo during wet season months in many semiarid regions, and strong variations of albedo within the Sahara Desert. These results will be further considered here using SSM/I polarization difference of brightness temperature at 19 GHz (PD19) and normalized difference vegetation index (NDVI) data to assess their validity.

NDVI represents the differential reflection of vegetation in the red and infrared channels of the National Oceanic and Atmosphere Administration (NOAA) polar orbiting satellites. It is most directly a measure of the photosynthetic capacity of the canopy and, roughly speaking, an indicator of the density of green vegetation, correlating well with such variables as leaf area index and vegetation cover.

PD19 is the difference of brightness temperature obtained from horizontally and vertically polarized radiation at 19 GHz, as measured by a pair of SSM/I radiometers. This difference is sensitive to surface properties. Becker and Choudhury (1988), for instance, have shown that the difference between polarized radiation in a microwave regime varies with vegetation density in marginal zones, such as Sahalian regions. This difference is also sensitive to soil moisture; an increase in soil moisture increases PD19. In contrast, the increase in vegetation density decreases PD19. Therefore, when rainfall occurs in semiarid regions (e.g., Sahel), one would expect an increase in PD19 due to higher soil moisture followed by a decrease in PD19 as the rainy season is established and as vegetation density increases.

Figure 10 displays a latitudinal transect (19°E) of surface albedo and PD19 for August 1987 and January 1988 and compares it with our values of surface albedo for these same months. A 5-yr average of surface albedo is also included. The dominant vegetation types along the 19°E transect are also indicated, based on White's (1983) vegetation map for Africa.

This section begins with a general discussion of the relationship between surface albedo and dominant surface vegetation type. Of particular interest is the seasonal albedo contrast in the various biomes. This is followed by a comparison of albedo and PD19 (section 7b) and a comparison of albedo and NDVI for select biomes (section 7c).

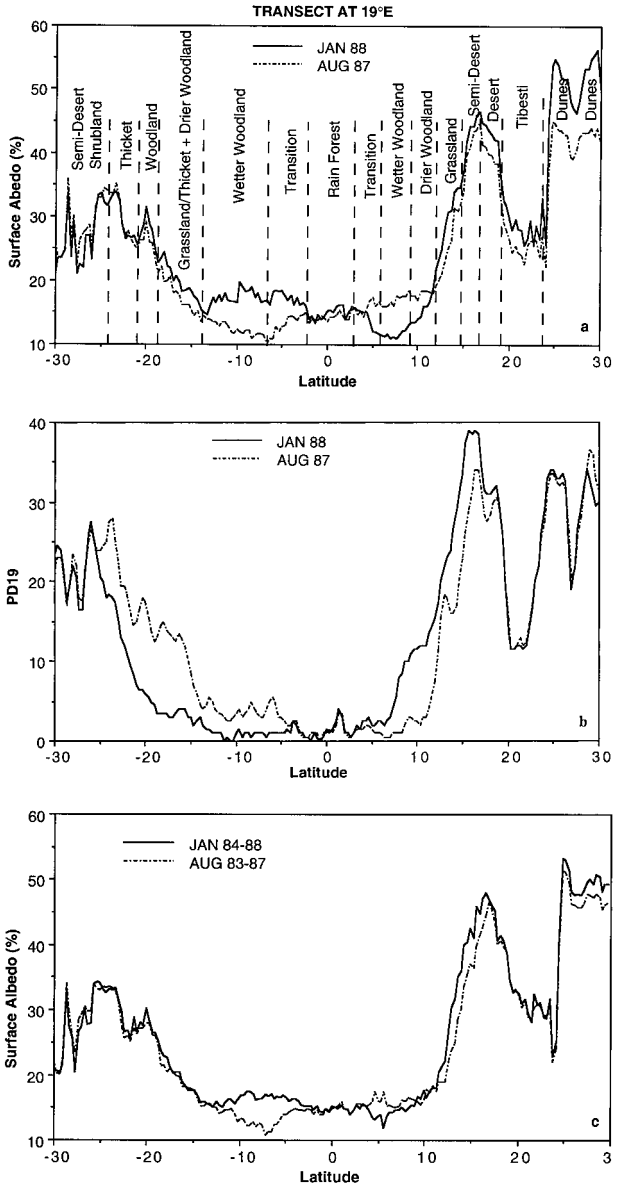

FIG. 10. (a) Latitudinal variations of surface albedo and (b) SSM/I polarization difference of brightness temperature at 19 GHz for Aug 1987 and Jan 1988 along a north–south transect at 19°E. (c) The long-term mean of surface albedo for Jan (1984–88) and Aug (1983–87) is also displayed. The dashed vertical lines delimit approximately the vegetation types (annotated) along the transects.

a. Albedo and surface vegetation

The vegetation types over Africa show a strong correspondence with features of the surface albedo (Fig. 10). In the region of tropical rain forest, surface albedo is low and shows little contrast between January and August. Further poleward, in the transition to the woodland and in the wetter woodland itself, a seasonal contrast becomes apparent, with higher albedo in the wetter season. The increase in foliage density might contribute to this seasonal change.

The higher albedo over the woodland in the wet season is clearly seen in the top diagram from the 1987–88 year. However, the seasonal cycle all but disappears in the Northern Hemisphere woodland in the mean for the years from 1983–84 to 1987–88. An examination of maps indicating surface hydrology shows that at 19°E, much of the woodland vegetation lies in swampland, which may reduce the seasonal growth cycle. The 1987 rainfall season was extremely dry in this region,

so the surface water may have dried up, producing seasonal dependence on local rainfall.

In the drier woodland and grassland, the albedo increases steadily with latitude, but seasonal contrast is reduced. Presumably, in this region the character of the surface and its reflective properties are imposed mainly by the presence of bare ground. The grassland in the Northern Hemisphere shows higher albedo during the dry season, a consequence of grasses covering the otherwise bare soil. In the equivalent vegetation zone of the Southern Hemisphere, there is higher albedo in the wet season. The reason for this is not readily apparent, but in this region, grassland is limited so that the thicket and woodland may determine most of the surface character. Also, the grassland there is edaphic, and thus growth may not be seasonal. It is further interesting to note the lower albedo over the thicket vegetation near 23°S and the high albedo of two dune fields near 26° and 29°N.

b. Relationship between surface albedo and polarization difference

Because surface albedo decreases with increasing soil moisture, identical patterns of PD19 and albedo are not to be anticipated, but several interesting points can be made from a comparison of the two parameters. Figure 10 displays a latitudinal transect (19°E) of (a) surface albedo and (b) PD19, respectively, for August 1987 and January 1988. Both surface albedo and PD19 show remarkable agreement, particularly over the desert regions along the polar extremes of the transect. This indicates the reality of the albedo maximum in the Southern Hemisphere at 22°–25°S and the relative minimum over the Sahara from about 18° to 24°N.

There is also substantial agreement in relatively small features in the PD19 and albedo fields over these deserts, suggesting that these are due to real differences in surface materials and soils. This is confirmed via maps of surface albedo and polarization difference for August 1987 (Fig. 11). Also, a comparison with a soils map shows that some of the structure of these fields over the drier regions can be directly related to soil differences.

Despite the relative agreement between surface albedo and PD19 for August, seasonal variations indicated by the two parameters show some significant contrasts. Both exhibit an absence of seasonal fluctuations near the equator and significant variations in those latitudes between the equatorial region and deserts, where there is a strong seasonal cycle in climatic conditions. However, PD19 shows no reversal in the sign of the seasonal cycle in the outer Tropics and quite different latitudes of maximum seasonal variations. PD19 and surface albedo are also in agreement over the Southern Hemisphere desert, but the patterns of seasonality are distinct over the Sahara. PD19 shows seasonally invariant values in contrast to strong seasonal variations in surface albedo over Sahara. This suggests that the albedo variations over Sahara are an artifact of the methodology.

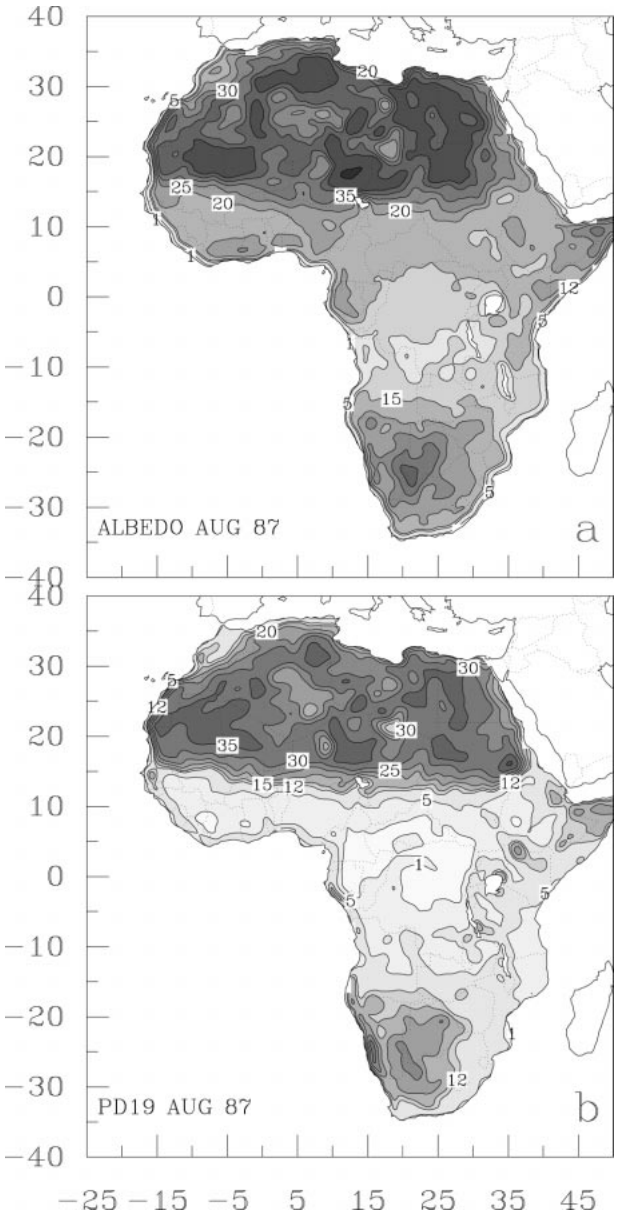

FIG. 11. Map of (a) mean surface albedo and (b) SSM/I polarization difference of brightness temperature at 19 Ghz for Aug 1987.

We suspect that the apparent seasonal variability of surface albedo in the southern Sahara (between August 1987 and January 1988) is produced by the seasonal fluctuations of atmospheric aerosols. Aerosol content in this region is lowest in July (N'Tchayi Mbourou et al. 1997) and is consistent with the relatively low albedo in July. It is also greatest in the central and southern Sahel, accounting for the greater seasonal contrasts in the 10°W transect at about 18°–22°N than in areas farther north. Furthermore, the seasonal variation over the central and southern desert is lower at 19°E than at 10°W

(see Fig. 5); this is consistent with the lower aerosol content over the eastern Sahara. When we considered a long-term monthly mean of surface albedo (January 1984–88 and August 1983–87), the seasonal variation is almost nonexistent over the northern Sahara (see Fig. 10c). Thus, the high values of surface albedo obtained in the northern Sahara during January 1988 is likely due to an anomalous high concentration of aerosols during that month.

The equatorial latitudes of minimal seasonal cycle correspond roughly to climates with year-round rainfall and equatorial forest biomes. The area farther poleward exhibits significant seasonal variations in both PD19 and surface albedo. Seasonal variations in albedo are greater in latitudes closest to the equatorial Tropics with subhumid climates and occupied by savanna woodlands. Seasonal variations in PD19 are greater in the outer-tropical latitudes with semiarid climates and savanna grasslands. This means that the seasonal cycle in PD19 reaches a maximum, where the influence of wetter soils and increasing vegetation cover of the wet season complement each other to maximize seasonal contrasts. Maximum seasonal variations in surface albedo occur where, during the wet season, the dense vegetation enhances albedo, but the wetter (and hence darker soil) is not exposed. Seasonal variations are lower in the drier regions, where during the dry season, the decrease in albedo due to reduced vegetation cover is counterbalanced by the comparatively high albedo of the exposed, dry soils.

c. Relationship between surface albedo and NDVI

Apparent in both Fig. 6 and Fig. 10 is a somewhat peculiar feature—a reversal of the seasonal cycle in albedo at about 10°N. This latitude approximately marks the transition from the savanna woodlands to the grasslands, with sparser vegetation cover. Our explanation for this feature is that in the woodlands, vegetation cover controls surface albedo, which increases as vegetation density increases. In the grasslands, with exposed soil during the dry season, the albedo reflects a combination of vegetation and soil reflectance and increases with increasing proportion of exposed bare soil (and hence increases during the dry season). An analysis of albedo and vegetation for various biomes of Africa suggests the validity of this interpretation.

Figure 12 shows cluster diagrams of surface albedo and NDVI during the wet and dry seasons for five general biomes: equatorial forest, forest/savanna transition, wet savanna woodlands, dry savanna woodlands, and savanna grasslands. These diagrams are produced by evaluating surface albedo and NDVI for individual stations in Africa and determining the vegetation at each station from White's (1983) vegetation map. There are separate analyses for the Northern and the Southern Hemispheres. Except in the equatorial latitudes, January (July) and July (January) represent the wet and dry seasons, respectively, in the Southern (Northern) Hemisphere.

In the wetter environments, there is a relatively small range of albedo and a comparatively large range of NDVI. This is true for the forest and transition biomes of the Northern Hemisphere and the forest, transition, and wetter woodland biomes of the Southern Hemisphere. In all but the forest biomes (where rainfall shows little seasonality), there is a small but discernible increase in both surface albedo and NDVI from the dry to the wet season. There is also a small increase of albedo with NDVI.

In the drier environments, the range of albedo becomes substantially larger. This is true for both woodlands and the grasslands in the Northern Hemisphere and for the drier woodland and the grassland in the Southern Hemisphere. The large range of surface albedo is particularly apparent in the dry seasons. This suggests that a fair amount of bare surface is exposed, with the properties of the soil influencing the albedo. In all of these biomes, NDVI is generally higher in the wet season, but surface albedo either bears no relationship to NDVI or it decreases with NDVI.

Earlier it was reasoned that the consistent association of higher albedo with the wet season throughout the Southern Hemisphere was a consequence of denser vegetation cover and less exposed bare ground. The denser vegetation cover is confirmed by the higher NDVI values in the Southern Hemisphere biomes in Fig. 12. The lower proportion of bare ground is confirmed by the lower scatter of surface albedo in the Southern Hemisphere biomes.

8. Conclusions

Overall, this study has demonstrated the complexity of the relationship between surface albedo and underlying surface conditions. For example, the albedo–vegetation relationship is different in dry regions than in wet ones. Some of the basic tenets of such issues as desertification or deforestation, such as the assumed increase in albedo as vegetation cover is reduced, are called into question. Our results also underscore the impact of soils on albedo in many of the dry regions.

The continental surface radiation balance derived by this study differs considerably from traditional climatological estimates. This throws into question much previous work on vegetation–climate relationships.

This study has further shown that the variability of atmospheric constituents, particularly aerosols, appears to introduce errors in the seasonal cycle and in year-to-year fluctuations. These problems must be overcome and radiometric calibration must be improved if satellite methods are to be used to study interannual variability of surface radiation balance on a continental scale. Despite this, it is clear that the seasonal and interannual variations of surface albedo within a climatic region are

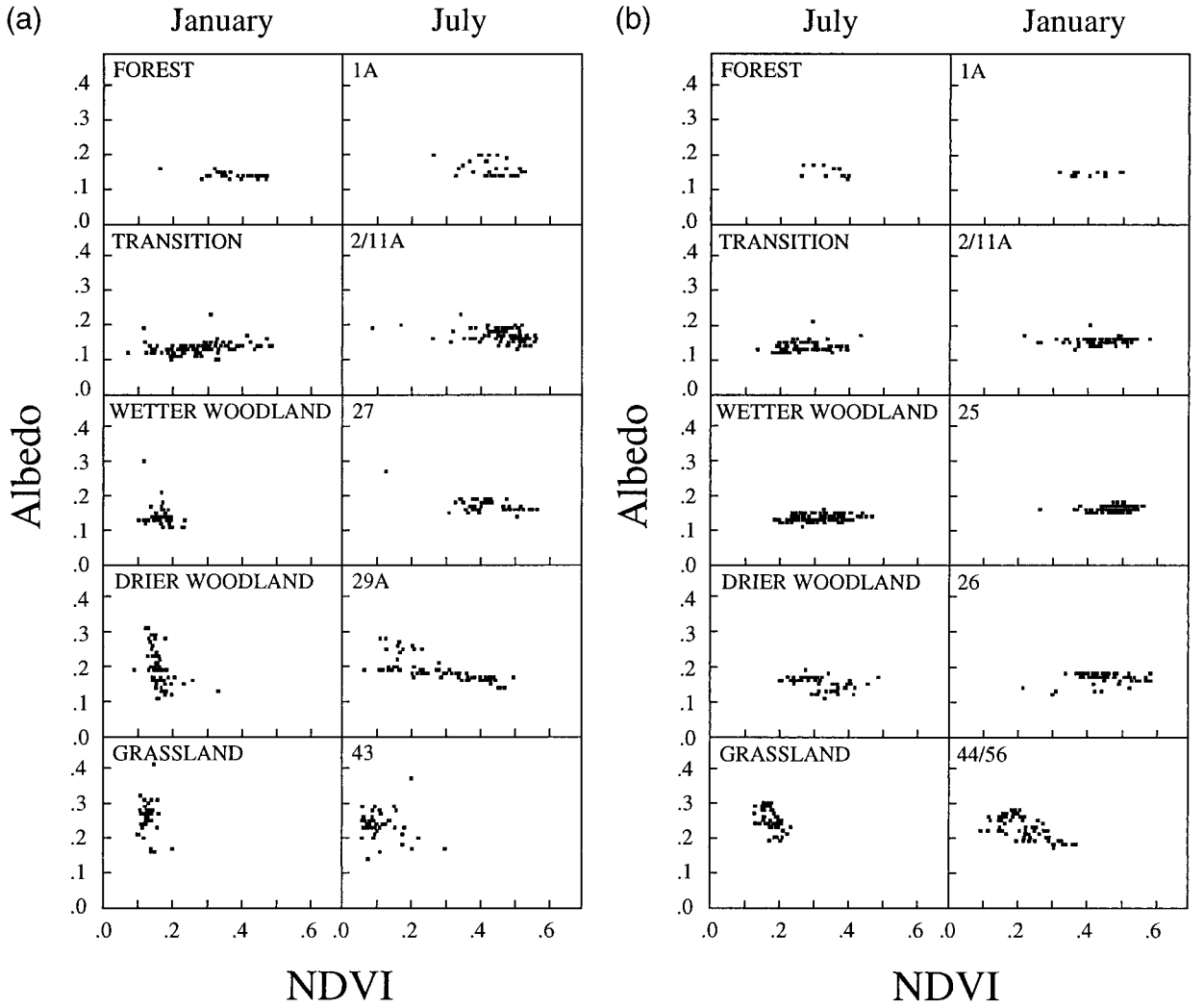

FIG. 12. Scatter diagrams of albedo and NDVI for various vegetation biomes in the (a) Northern Hemisphere (NH) and (b) Southern Hemisphere (SH) of Africa. The wet season is represented by Jan in the SH, Jul in the NH; the dry season is Jul in the SH, Jan in the NH. Numbers indicate the biome number according to White's (1983) map.

relatively small when compared with the contrast between regions of diverse climate.

Acknowledgments. We would like to thank Mr. J. Kim of the Florida State University for programming support and Dr. N. Grody at NOAA/NESDIS, Camp Springs, MD, for useful discussions on the physical interpretation of SSM/I measurements. Longwave radiation data used in the study were obtained from NASA/Langley Research Center Distributed Active Archive Center. The NDVI data were obtained from Dr. C. J. Tucker of NASA Goddard Space Flight Center, Greenbelt, Maryland. This work was sponsored by the NASA TRMM project under NASA Grant NAG5-1587. Florida State University provided some support for the participation of S. Nicholson. Dr. Frouin was supported by NASA under Grant NAGW-2727 and by the California Space Institute.

REFERENCES

Ba, M. B., R. Frouin, S. E. Nicholson, and G. Dedieu, 2001: Satellite-derived surface radiation budget over the African continent. Part I: Estimation of downward solar irradiance and albedo. *J. Climate*, **14,** 45–58.

Becker, F. B. G., and B. Choudhury, 1988: Relative sensitivity of normalized difference index (NDVI) and microwave polarization difference index (MPDI) for vegetation and desertification monitoring. *Remote Sens. Environ.*, **24,** 297–312.

Budyko, M. I., 1986: *The Evolution of the Biosphere.* Reidel, 423 pp.

Charney, J. G., 1975: Dynamics of deserts and droughts in the Sahel. *Quart. J. Roy. Meteor. Soc.*, **101,** 193–202.

Courel, M. F., R. S. Kandel, and S. I. Rasool, 1984: Surface albedo and the Sahel drought. *Nature*, **307,** 528–531.

Darnell, W. L., W. F. Staylor, S. K. Gupta, N. A. Ritchey, and A. C. Wilber, 1992: Seasonal variation of surface radiation budget derived from International Satellite Cloud Climatology Project C1 data. *J. Geophys. Res.*, **97,** 15 741–15 760.

Deschamps, P. Y., and G. Dedieu, 1986: Comments on ''Surface al-

bedo over the Sahel from METEOSAT radiances.'' *J. Climate Appl. Meteor.,* **25,** 575–576.
Dickinson, R. E., 1983: Land surface processes and climate-surface albedos and energy balance. *Advances in Geophysics,* Vol. 25, Academic Press, 305–353.
FAO, 1977: *Soil Map of the World.* Vol. VI. *Africa.* UNESCO, 218 pp.
Flohn, H., 1971: Tropische Zirkulations—Formen in Lichte de Satellitenaufnahmen. *Bonner Meteor. Abhandlungen,* **5,** 57 pp.
Gupta, S. K., N. A. Ritchey, A. C. Wilber, C. H. Whitlock, G. G. Gibson, and P. W. Stackhouse Jr., 1999: A climatology of surface radiation budget derived from satellite data. *J. Climate,* **12,** 2689–2708.
Henning, D., 1989: *Atlas of the Surface Heat Balance of the Continents.* Gebrueder Borntraeger, 402 pp.
Lancaster, N., 1996: Deserts. *The Physical Geography of Africa,* A. S. Goudie, W. M. Adams, and A. Orme, Eds., Oxford University Press, 211–237.
Lare, A. R., and S. E. Nicholson, 1990: A climatonomic description of the surface energy balance in the central Sahel. Part I: Shortwave radiation. *J. Appl. Meteor.,* **29,** 123–137.
Leroux, X., J. Polcher, G. Dedieu, J. C. Menaut, and B. Monteny, 1994: Radiation exchanges above west African moist savannas: Seasonal patterns, and comparison with a GCM simulation. *J. Geophys. Res.,* **99,** 25 857–25 868.
Li, Z., and L. Garand, 1994: Estimation of surface albedo from space: A parameterization for global application. *J. Geophys. Res.,* **99,** 8335–8350.
London, J., R. D. Bojkov, S. Oltmans, and J. I. Kelley, 1976: Atlas of the global distribution of total ozone July 1957–June 1967. National Center for Atmospheric Research Tech. Note 113+STR, University Corporation for Atmospheric Research, Boulder, CO, 276 pp.
Nicholson, S. E., 1981: Rainfall and atmospheric circulation during drought periods and wetter years in West Africa. *Mon. Wea. Rev.,* **109,** 2191–2208.
——, and T. J. Farrar, 1994: The influence of soil type on the relationships between NDVI, rainfall, and soil moisture in semiarid Botswana. I. NDVI response to rainfall. *Remote Sens. Environ.,* **50,** 107–120.
Norton, C. C., F. R. Mosher, and B. Hinton, 1979: An investigation of surface albedo variations during the recent Sahel drought. *J. Appl. Meteor.,* **18,** 1252–1262.
N'Tchayi Mbourou, G., J. Bertrand, and S. E. Nicholson, 1997: The diurnal and seasonal cycles of wind-borne dust over Africa north of the equator. *J. Appl. Meteor.,* **36,** 868–882.
Pinker, R. T., and I. Laszlo, 1992: Modeling surface solar irradiance for satellite applications on a global scale. *J. Appl. Meteor.,* **31,** 194–211.
Pinty, B., and G. Szejwach, 1985: A new technique for inferring surface albedo from satellite observations. *J. Climate Appl. Meteor.,* **24,** 741–750.
——, and D. Ramond, 1987: A method for estimate of broadband directional surface albedo from a geostationary satellite. *J. Climate Appl. Meteor.,* **26,** 1709–1722.
——, and D. Tanré, 1987: The relationship between incident and double-way transmittances: An application for the estimate of surface albedo from satellites over the African Sahel. *J. Climate Appl. Meteor.,* **26,** 892–896.
——, ——, and J. Stum, 1985: Surface albedo over the Sahel from METEOSAT radiances. *J. Climate Appl. Meteor.,* **24,** 108–113.
Rockwood, A. A., and S. K. Cox, 1978: Satellite inferred surface albedo over northwestern Africa. *J. Atmos. Sci.,* **35,** 513–522.
Tanré, D., C. Deroo, P. Duhaut, M. Herman, J. J. Morcrette, J. Perbos, and P. Y. Deschamps, 1990: Description of computer code to simulate the satellite signal in the solar spectrum: The 5S code. *Int. J. Remote Sens.,* **11,** 659–668.
Tuller, S. E., 1968: World distribution of mean monthly and annual precipitable water. *Mon. Wea. Rev.,* **96,** 785–797.
White, F., 1983: *The Vegetation of Africa.* UNESCO, 383 pp.